Magnetoinductive Waves and Complex Modes in Two-Dimensional Periodic Arrays of Split Ring Resonators

Salvatore Campione, *Student Member, IEEE*, Francisco Mesa, *Senior Member, IEEE*, and Filippo Capolino, *Senior Member, IEEE*

***Abstract*—We investigate magnetoinductive waves in two-dimensional periodic arrays of split ring resonators or capacitively loaded loops and characterize the modes with real and complex wavenumber excitable in such arrays. Each resonator is modeled as a single magnetic dipole, and the computation of the modal wavenumbers is performed by searching for the zeroes of the homogeneous scalar equation characterizing the field in the array. We provide original developments for the Ewald method applied to the required dyadic periodic Green's function for the array of magnetic dipoles, including the quasi-static case. The Ewald representation is analytically continued into the complex wavenumber space and also provides series with Gaussian convergence rate. In particular, we analyze and classify proper, improper, forward, backward, bound, and leaky magnetoinductive waves varying frequency and compare the fully retarded solution to the quasi-static one. We highlight the importance of accounting for field retardation effects for the prediction of the physical waves excitable in the array when the dimensions of its unit cell are approximately greater than a tenth of the free-space wavelength. The proposed method complements previous investigations and is a powerful tool for the design of waveguiding or radiating structures based on magnetoinductive waves.**

***Index Terms*—Magnetoinductive waves, metamaterials, modal analysis, split ring resonators.**

I. Introduction

MAGNETICALLY coupled resonators can support propagating waves, which are generally referred to as *magnetoinductive* (MI) waves. The simplest set of resonators consists of a capacitor and an inductor coupled with other resonators of the same kind, which can be easily realized with capacitively loaded loops or split ring resonators (SRRs), as shown in the inset in Fig. 1. These resonators may be for example used to achieve left-handed metamaterials [1], effective negative permeability [2], and tunable metamaterial components [3].

Manuscript received December 15, 2012; revised March 08, 2013; accepted April 06, 2013. Date of publication April 16, 2013; date of current version July 01, 2013. The work of S. Campione and F. Capolino has been supported in part by the National Science Foundation under Grant No. CMMI-1101074. The work of F. Mesa has been supported by the Spanish Ministerio de Ciencia e Innovación and European Union FEDER funds (project TEC2010-16948) and by Consolider CSD2008-00066.

S. Campione and F. Capolino are with the Department of Electrical Engineering and Computer Science, University of California Irvine, Irvine CA 92697 USA (e-mail: scampion@uci.edu; f.capolino@uci.edu).

F. Mesa is with the Department of Applied Physics 1, ETS de Ingenieria Informatica, University of Seville, Seville 41012 Spain (e-mail: mesa@us.es).

Color versions of one or more of the figures in this paper are available online at http://ieeexplore.ieee.org.

Digital Object Identifier 10.1109/TAP.2013.2258395

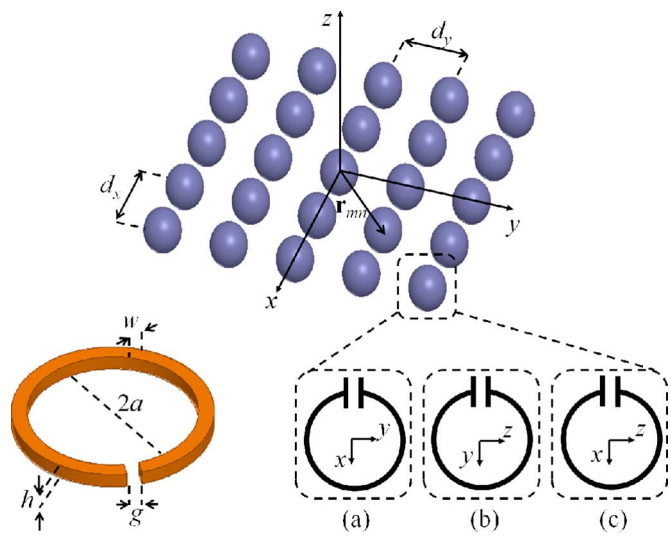

Fig. 1. Two-dimensional periodic array of capacitively loaded loops or SRRs displaced in the x–y plane with ring plane in the (a) x–y, (b) y–z, and (c) x–z plane, embedded in a homogeneous environment with relative permittivity ε_h. The 00th reference resonator is placed here at $\mathbf{r}_{00} = \mathbf{0}$, and d_x and d_y are the periodicities along the x- and y- directions, respectively.

Moreover, applications of MI waves include near-field imaging [4]–[8] and data transfer channels [9], for example.

Magnetoinductive waves have been studied in arrays of SRRs periodic in one (1D), two (2D), or three dimensions in [10] by using a circuit formulation, taking into account the coupling between elements and neglecting retardation (i.e., the dimensions of the structure are assumed to be small with respect to the free space wavelength). The authors in [10] have shown that the nearest neighbor approximation provides the salient propagation features and that more coupling with further resonators is needed for higher accuracy of the results. The propagation in linear arrays of SRRs in axial or transverse configuration (i.e., the wavevector is in the same direction or in the transverse direction of the magnetic dipole moment describing the SRR, respectively) has been studied experimentally in [11], and similar works (including theory) have been shown in [12]–[15]. The dispersion properties of a bi-periodic linear array of SRRs (contiguous loops are loaded with different capacitances) have been shown experimentally in [16] to support MI waves in two distinct frequency bands. The same phenomenon has been studied thoroughly in linear arrays in [17] for a unit cell with two SRRs whose relative distance is smaller than the period. The arranging in various orientations of the SRRs in two coupled linear arrays

to tailor the dispersion diagrams has been shown in [18]. Experimental and theoretical analyses of the coupling mechanisms between contiguous SRRs have been shown in [19], where it is stated that, depending on the relative orientation of the SRRs, the coupling may be either of magnetic or electric type or a combination of the two; this fact can allow, for example, the design of nanostructured devices based on propagation of slow waves. The dispersion equations of finite linear arrays made of coupled SRRs and plasmonic nanoparticles have been retrieved in [20] when the interelement coupling is governed by retardation effects, showing how the two are closely related to each other. The transmission and reflection properties of a left-handed metamaterial made of 2D arrays of SRRs or wires have been shown in [21]. A comprehensive review of MI wave theory and applications has been also provided in [22] and [23]. Propagating and evanescent waves for 2D periodic structures have been studied in [24] by adding eight new zones to the traditional first Brillouin zone, which have allowed to include in graphical form the full information contained in a lossless dispersion equation. Magnetostatic spin waves and their wavenumber-frequency dispersion diagrams have also been studied in linear arrays of ferromagnetic nanowires [25]. Very recently, magnetoinductive polaritons, defined as hybrid polaritonic modes of electromagnetic waves and of slow waves of coupling between resonators, have been introduced in [26], which have allowed for the design of structures with controllable effective material parameters and with required functionality (e.g., realization of Pendry's near-perfect lens).

The aim of this paper is to characterize the bound (non radiating) and leaky (radiating) modes with real and complex wavenumber excitable in 2D periodic arrays of SRRs (Fig. 1), was recently done in [27] and [28] for 1D and 2D periodic arrays of plasmonic nanoparticles. In Section II, we model each SRR as a single magnetic dipole through the single dipole approximation (SDA) [29], [30] and use a periodic Green's function (GF) formulation based on the Ewald method (outlined in Section III) to describe the field in the array, as shown in [28] and [31]. We then obtain in Section IV reflection and transmission coefficients of an array of SRRs in the gigahertz range under oblique TE-polarized plane wave incidence and characterize the modes excitable in the same array. Modal analysis in an array of capacitively loaded loops in the megahertz range is performed in Section V for different loop orientations. The two numerical analyses in Sections IV and V are intended to confirm that our method provides results in good agreement with full-wave results and may be applied to any frequency range and thus employed for the design of waveguiding or radiating structures based on magnetoinductive waves. The analysis in this paper is a necessary step towards a thorough understanding of modal description in periodic arrays, and specifically the characterization of MI waves. In this regard, this paper also presents a number of novel discussions and numerical results.

II. Dynamic Simulation Model Including All Couplings

A. Periodic Green's Function for the Evaluation of the Modal Wavenumbers

The structure under analysis is the 2D periodic array of SRRs (or capacitively loaded loops) reported in Fig. 1. The monochromatic time harmonic convention $\exp(j\omega t)$ is assumed here and throughout the paper, and is therefore suppressed hereafter. Here, bold fonts refer to vector quantities, a bar under a bold letter refers to dyadic quantities, and a hat denotes unit vectors.

We model each SRR as a single magnetic dipole. This is a good approximation when the magnetic dipolar term dominates the scattered-field multipole expansion, which is likely to happen when the SRR dimensions are much smaller than the incident wavelength, and when the periods $d_x, d_y \geq 3a$. Note that fairly accurate results may still be obtained even for smaller periods. As such, the induced magnetic dipole moment $\mathbf{m}$ is given by

$$\mathbf{m} = \underline{\boldsymbol{\alpha}}_{\mathrm{m}} \cdot \mathbf{H}^{\mathrm{loc}} \tag{1}$$

where $\underline{\boldsymbol{\alpha}}_{\mathrm{m}}$ is the dyadic magnetic polarizability of the SRR, and $\mathbf{H}^{\mathrm{loc}}$ is the local magnetic field produced by all the SRRs of the array except the considered SRR, plus the external incident field to the array, if present. An SRR has an anisotropic magnetic polarizability directed along the direction orthogonal to the ring plane, denoted here as $\hat{\mathbf{v}}$, which in this paper coincides either with $\hat{\mathbf{x}}, \hat{\mathbf{y}}$, or $\hat{\mathbf{z}}$. Accordingly, the SRR dyadic magnetic polarizability is given by $\underline{\boldsymbol{\alpha}}_{\mathrm{m}} = \hat{\mathbf{v}}\hat{\mathbf{v}}\alpha_{\mathrm{m}}$, where the quasi-static expression for α_{m} is given by [32]–[34]

$$\alpha_{\mathrm{m}} = \left\{ \frac{1}{\alpha'_{\mathrm{m}}} + j\frac{k^3}{6\pi} \right\}^{-1} \tag{2}$$

with

$$\alpha'_{\mathrm{m}} = \mu_0 \frac{A^2}{L} \left(\frac{\omega_0^2}{\omega^2} - 1 + j\frac{R_l}{\omega L} \right)^{-1}. \tag{3}$$

In the above expressions, $\mu_0 = 4\pi \times 10^{-7}$ H/m is the permeability of free space, $A = \pi a^2$ is the area of the ring,

$$L = \mu_0 a \left[\ln\left(16\frac{a}{w}\right) - 2 \right] \tag{4}$$

is the self-inductance of a perfectly conducting ring [32], with a and w ($w \ll a$) denoting the radius and the width of the ring (Fig. 1). Moreover, $\omega_0 = 1/\sqrt{LC}$ is the resonance angular frequency of the ring after having applied the capacitive split or a lumped capacitor C, and $R_l \approx R_S \pi a/(w+h)$ accounts for the metal losses, with h the thickness of the ring, and $R_S = \sqrt{\omega\mu_0/(2\sigma)}$ the surface resistance, which depends only on the constitutive material of the ring (σ is the metal conductivity). The quality factor of the ring series resonance, evaluated at the resonance frequency and neglecting radiation losses, is given by $Q = \sqrt{L/C}/R_l$. The term $jk^3/(6\pi)$ in (2) is added to account for radiation damping in order to satisfy the energy conservation law [35] and $k = k_0\sqrt{\varepsilon_h}$ is the host wavenumber, with k_0 the free-space wavenumber and ε_h the host relative permittivity.

Consider now a 2D periodic array of SRRs located in the x–y plane as in Fig. 1, with the rings plane in the x–y [Fig. 1(a)], y–z [Fig. 1(b)], or x–z [Fig. 1(c)] plane, immersed in a homogeneous background with relative permittivity ε_h. Each SRR is placed at positions $\mathbf{r}_{mn} = \mathbf{r}_{00} + \mathbf{d}_{mn}$, where $\mathbf{d}_{mn} = md_x\hat{\mathbf{x}} + nd_y\hat{\mathbf{y}}$, with $m, n = 0, \pm1, \pm2, \ldots$, $\mathbf{r}_{00} = x_{00}\hat{\mathbf{x}} + y_{00}\hat{\mathbf{y}} + z_{00}\hat{\mathbf{z}}$, and d_x and d_y are the periodicities along the x- and y-directions, respectively [28], [29].

Suppose that the array is either excited by a plane wave or supports a mode. In both cases, the field is periodic, except for a phase shift described by the Bloch wavevector $\mathbf{k}_{\mathrm{B}} = k_x\hat{\mathbf{x}} + k_y\hat{\mathbf{y}}$, which also accounts for decay in case the wavenumbers are complex. Consequently, the mnth SRR is represented by a magnetic dipole moment equal to $\mathbf{m}_{mn} = \mathbf{m}_{00}\exp(-j\mathbf{k}_{\mathrm{B}} \cdot \mathbf{d}_{mn})$,

where $\mathbf{m}_{00}$ represents the magnetic dipole moment of the 00th reference SRR. The local magnetic field acting on the reference SRR at position $\mathbf{r}_{00}$ is given by

$$\mathbf{H}^{\mathrm{loc}}(\mathbf{r}_{00},\mathbf{k}_{\mathrm{B}}) = \mathbf{H}^{\mathrm{inc}}(\mathbf{r}_{00}) + \breve{\underline{\mathbf{G}}}^{\infty}(\mathbf{r}_{00},\mathbf{r}_{00},\mathbf{k}_{\mathrm{B}})\cdot\mathbf{m}_{00} \quad (5)$$

where $\mathbf{H}^{\mathrm{inc}}$ is the incident magnetic field, and $\breve{\underline{\mathbf{G}}}^{\infty}(\mathbf{r}_{00},\mathbf{r}_{00},\mathbf{k}_{\mathrm{B}})$ accounts for all the mutual couplings between all mn-indexed magnetic dipoles and $\mathbf{m}_{00}$, and therefore it is not singular at $\mathbf{r}=\mathbf{r}_{00}$. The term $\breve{\underline{\mathbf{G}}}^{\infty}$ is the regularized periodic dyadic GF, defined as $\breve{\underline{\mathbf{G}}}^{\infty}(\mathbf{r},\mathbf{r}_{00},\mathbf{k}_{\mathrm{B}}) = \underline{\mathbf{G}}^{\infty}(\mathbf{r},\mathbf{r}_{00},\mathbf{k}_{\mathrm{B}}) - \underline{\mathbf{G}}(\mathbf{r},\mathbf{r}_{00})$, where

$$\underline{\mathbf{G}}^{\infty}(\mathbf{r},\mathbf{r}_{00},\mathbf{k}_{\mathrm{B}}) = \sum_{m,n=-\infty}^{+\infty}\underline{\mathbf{G}}(\mathbf{r},\mathbf{r}_{mn})e^{-j\mathbf{k}_{\mathrm{B}}\cdot\mathbf{d}_{mn}} \quad (6)$$

is the magnetic-field dyadic GF for the phased "infinite" periodic array of magnetic dipoles. Here, $\underline{\mathbf{G}}(\mathbf{r},\mathbf{r}')$ denotes the dyadic GF for a single magnetic dipole in the homogeneous background

$$\underline{\mathbf{G}}(\mathbf{r},\mathbf{r}') = \frac{e^{-jkR}}{4\pi}\left[\left(\frac{k^2}{R}-\frac{jk}{R^2}-\frac{1}{R^3}\right)\underline{\mathbf{I}} - \left(\frac{k^2}{R}-\frac{3jk}{R^2}-\frac{3}{R^3}\right)\hat{\mathbf{R}}\hat{\mathbf{R}}\right] \quad (7)$$

where $\mathbf{R}=R\hat{\mathbf{R}}=\mathbf{r}-\mathbf{r}'$ is the vector from the source at $\mathbf{r}'$ to the observer at $\mathbf{r}$, $R=|\mathbf{r}-\mathbf{r}'|$, and $\underline{\mathbf{I}}$ is the identity dyad. The expression in (7) includes all field retardation (FR) effects. In this paper we also consider the case where the magnetic dipoles emit only magnetic fields according to the quasi-static (QS) model

$$\underline{\mathbf{G}}(\mathbf{r},\mathbf{r}') \approx \frac{1}{4\pi R^3}[-\underline{\mathbf{I}}+3\hat{\mathbf{R}}\hat{\mathbf{R}}] \quad (8)$$

which is a good approximation when the SRR radius and the periods d_x and d_y are all much smaller than the wavelength, at any distance such that $kR \ll 1$.

Independently of the adopted GF (the one with FR effects or the QS approximation), substituting the expression for the local field in (5) into (1) and assuming a specific SRR axis orientation along a predetermined direction $v = x, y$, or z, one obtains $\mathbf{m}_{00}=\hat{\mathbf{v}}\,m_{00}$, where m_{00} satisfies the scalar equation $m_{00} = \alpha_{\mathrm{m}}H_v^{\mathrm{inc}}(\mathbf{r}_{00}) + \alpha_{\mathrm{m}}\breve{G}^{\infty}_{\mathrm{vv}}(\mathbf{r}_{00},\mathbf{r}_{00},\mathbf{k}_{\mathrm{B}})m_{00}$, with $\breve{G}^{\infty}_{\mathrm{vv}}$ being the proper diagonal component of the 2D periodic regularized dyadic GF and $H_v^{\mathrm{inc}}=\hat{\mathbf{v}}\cdot\mathbf{H}^{\mathrm{inc}}$. This leads to the scalar equation

$$A_{\mathrm{vv}}(\mathbf{k}_{\mathrm{B}})m_{00} = \alpha_{\mathrm{m}}H_v^{\mathrm{inc}}(\mathbf{r}_{00}) \quad (9)$$

where

$$A_{\mathrm{vv}}(\mathbf{k}_{\mathrm{B}}) = 1-\alpha_{\mathrm{m}}\breve{G}^{\infty}_{\mathrm{vv}}(\mathbf{r}_{00},\mathbf{r}_{00},\mathbf{k}_{\mathrm{B}}). \quad (10)$$

Mode analysis in the 2D periodic array is performed by computing the zeroes of the homogeneous version of (9); i.e., when no impressed excitation is present. This requires, in general, the solving of $A_{\mathrm{vv}}(\mathbf{k}_{\mathrm{B}})=0$ for complex $\mathbf{k}_{\mathrm{B}}$. Due to symmetry both $\pm\mathbf{k}_{\mathrm{B}}$ are solutions. In the lossless case also $\pm\mathbf{k}_{\mathrm{B}}^*$ would be solutions, where the $*$ denotes complex conjugate. However, in the present case where some losses are present but are not very large, if $\mathbf{k}_{\mathrm{B}}$ is a solution, in general a solution near $\mathbf{k}_{\mathrm{B}}^*$ may be found.

B. Floquet Waves Representation and Physical Excitation Conditions

As mentioned in Section II-A, the magnetic field in the planar array is periodic except for a phase shift, that is $\mathbf{H}(\mathbf{r}+\mathbf{d}_{mn},\mathbf{k}_{\mathrm{B}}) = \mathbf{H}(\mathbf{r},\mathbf{k}_{\mathrm{B}})\exp(-j\mathbf{k}_{\mathrm{B}}\cdot\mathbf{d}_{mn})$, with $\mathbf{r}=x\hat{\mathbf{x}}+y\hat{\mathbf{y}}+z\hat{\mathbf{z}}$. The field relative to a mode in the array is expressed in terms of Floquet waves as

$$\mathbf{H}^{\mathrm{mode}}(\mathbf{r},\mathbf{k}_{\mathrm{B}}) = \sum_{p,q=-\infty}^{+\infty}\mathbf{h}_{pq}^{\mathrm{mode}}(z,\mathbf{k}_{\mathrm{B}})e^{-j(k_{x,p}x+k_{y,q}y)} \quad (11)$$

where $k_{x,p}=k_x+2\pi p/d_x=\beta_{x,p}-j\alpha_x$, $k_{y,q}=k_y+2\pi q/d_y=\beta_{y,q}-j\alpha_y$, and $\mathbf{h}_{pq}^{\mathrm{mode}}$ is the weight of the pqth harmonic. The real parts $\beta_{x,p}$ and $\beta_{y,q}$ are repeated periodically in the complex wavenumber domain, with periods $2\pi p/d_x$ and $2\pi q/d_y$, respectively. Due to this period, a mode will be described by the wavenumber of its Floquet wave in the fundamental Brillouin zone (BZ), defined as $-\pi/d_x<\beta_{x,0}<\pi/d_x$ and $-\pi/d_y<\beta_{y,0}<\pi/d_y$. Therefore here, by definition, the wavenumbers k_x and k_y lie in the fundamental BZ. Furthermore, the vertical wavenumber is $k_{z,pq}=\sqrt{k^2-\mathbf{k}_{t,pq}\cdot\mathbf{k}_{t,pq}}=\beta_{z,pq}-j\alpha_{z,pq}$, with $\mathbf{k}_{t,pq}=k_{x,p}\hat{\mathbf{x}}+k_{y,q}\hat{\mathbf{y}}$. We distinguish between proper (i.e., decaying getting away from the array, $\mathrm{Im}(k_{z,pq})<0, \alpha_{z,pq}>0$) and improper (i.e., growing getting away from the array, $\mathrm{Im}(k_{z,pq})>0, \alpha_{z,pq}<0$) harmonics as previously done in [28], and also described in [36] and [37]. This classification provides us with the knowledge of the physical bound and leaky modes excitable in the array. By *physical*, we mean those that can be excited by a localized source, a defect, or array truncation. Modes that are not classified as physical here may, however, be excited by much more complicated source distributions, though this study is not within the scope of this paper.

Among all the mathematical solutions of $A_{\mathrm{vv}}(\mathbf{k}_{\mathrm{B}})=0$ [as dictated by (9) as discussed in Section II-A], only a subset represents physical waves. These are summarized in Table I based on the complex wavenumber of the fundamental Floquet harmonic in the first BZ (i.e., the one with $p=0$ and $q=0$), assuming $k_y=0$. Modes are classified as backward when $\beta_{x,0}\alpha_x<0$ and forward when $\beta_{x,0}\alpha_x>0$; bound when $|\beta_{x,0}|>k$ (slow wave) and leaky when $|\beta_{x,0}|<k$ (fast wave). The periodic condition $k_{x,p}=k_x+2\pi p/d_x$ would determine the behavior of Floquet harmonics with wavenumbers in other BZs. Note that in the case of array periods shorter than half wavelength, only wavenumbers in the fundamental BZ may represent fast waves. For larger periods, the leaky wavenumbers in the fundamental BZ may originate from higher order harmonics, as it happens, for example, in leaky wave antennas whose radiation is coming from the -1 Floquet harmonic [38].

III. Ewald Representation for the Dyadic Green's Function for 2D Periodic Arrays of Magnetic Dipoles

The Ewald representation for the 2D periodic regularized dyadic GF, $\breve{\underline{\mathbf{G}}}^{\infty}$, used in (5), can be evaluated following the derivations in [28] and [31] adapted here to the array of magnetic dipoles. We take full advantage of the duality principle,

TABLE I
CLASSIFICATION OF PHYSICAL MODES WITH COMPLEX WAVENUMBER OF THE FUNDAMENTAL FLOQUET HARMONIC, ASSUMING $k_y = 0$

	Forward wave $\beta_{x,0}\alpha_x > 0$	**Backward wave** $\beta_{x,0}\alpha_x < 0$
Slow wave $\lvert\beta_{x,0}\rvert > k$	$\alpha_{z,00} > 0$ Proper, bound	$\alpha_{z,00} > 0$ Proper, bound
Fast wave $\lvert\beta_{x,0}\rvert < k$	$\alpha_{z,00} < 0$ Improper, leaky	$\alpha_{z,00} > 0$ Proper, leaky

and accordingly, $\breve{\underline{\mathbf{G}}}^{\infty}$ is split into the hybrid sum of spectral and spatial terms as

$$\breve{\underline{\mathbf{G}}}^{\infty}(\mathbf{r},\mathbf{r}_{00},\mathbf{k}_{\mathrm{B}}) = \underline{\mathbf{G}}^{\infty}_{\mathrm{spectral}}(\mathbf{r},\mathbf{r}_{00},\mathbf{k}_{\mathrm{B}}) + \breve{\underline{\mathbf{G}}}^{\infty}_{\mathrm{spatial}}(\mathbf{r},\mathbf{r}_{00},\mathbf{k}_{\mathrm{B}}) \tag{12}$$

with

$$\underline{\mathbf{G}}^{\infty}_{\mathrm{spectral}}(\mathbf{r},\mathbf{r}_{00},\mathbf{k}_{\mathrm{B}}) = [k^2\underline{\mathbf{I}} + \nabla\nabla]G^{\infty}_{\mathrm{spectral}}(\mathbf{r},\mathbf{r}_{00},\mathbf{k}_{\mathrm{B}}), \tag{13}$$

$$\breve{\underline{\mathbf{G}}}^{\infty}_{\mathrm{spatial}}(\mathbf{r},\mathbf{r}_{00},\mathbf{k}_{\mathrm{B}}) = [k^2\underline{\mathbf{I}} + \nabla\nabla]\breve{G}^{\infty}_{\mathrm{spatial}}(\mathbf{r},\mathbf{r}_{00},\mathbf{k}_{\mathrm{B}}). \tag{14}$$

The scalar terms in (13)–(14) are given by

$$G^{\infty}_{\mathrm{spectral}}(\mathbf{r},\mathbf{r}_{00},\mathbf{k}_{\mathrm{B}}) = \frac{1}{4jd_xd_y}\sum_{p,q=-\infty}^{+\infty}\frac{f_{pq}(z-z_{00})}{k_{z,pq}}e^{-j\mathbf{k}_{t,pq}\cdot(\mathbf{r}-\mathbf{r}_{00})} \tag{15}$$

with $\mathbf{k}_{t,pq} = \mathbf{k}_{\mathrm{B}} + (2\pi p/d_x)\hat{\mathbf{x}} + (2\pi q/d_y)\hat{\mathbf{y}}$, and

$$\breve{G}^{\infty}_{\mathrm{spatial}}(\mathbf{r},\mathbf{r}_{00},\mathbf{k}_{\mathrm{B}}) = \breve{G}^{\infty}_{00} + \frac{1}{8\pi}\sum_{\substack{m,n=-\infty\\ m,n\neq 0}}^{+\infty}\frac{f(R_{mn})}{R_{mn}}e^{-j\mathbf{k}_{\mathrm{B}}\cdot\mathbf{r}_{mn}} \tag{16}$$

and their derivation is sketched in Appendix A. Moreover,

$$\nabla\nabla G^{\infty}_{\mathrm{spectral}}(\mathbf{r},\mathbf{r}_{00},\mathbf{k}_{\mathrm{B}}) = \frac{-1}{4jd_xd_y}\times\sum_{p,q=-\infty}^{+\infty}\frac{\underline{\mathbf{F}}_{\mathrm{spectral}}(z-z_{00})}{k_{z,pq}}e^{-j\mathbf{k}_{t,pq}\cdot(\mathbf{r}-\mathbf{r}_{00})} \tag{17}$$

and

$$\nabla\nabla\breve{G}^{\infty}_{\mathrm{spatial}}(\mathbf{r},\mathbf{r}_{00},\mathbf{k}_{\mathrm{B}}) = \nabla\nabla\breve{G}^{\infty}_{00} + \frac{1}{8\pi}\sum_{\substack{m,n=-\infty\\ m,n\neq 0}}^{+\infty}\underline{\mathbf{F}}_{\mathrm{spatial}}(R_{mn})e^{-j\mathbf{k}_{\mathrm{B}}\cdot\mathbf{r}_{mn}}. \tag{18}$$

This representation applies to both the FR and QS cases. For the FR case, the expressions for $f_{pq}, f, \breve{G}^{\infty}_{00}, \underline{\mathbf{F}}_{\mathrm{spectral}}, \underline{\mathbf{F}}_{\mathrm{spatial}}$ and $\nabla\nabla\breve{G}^{\infty}_{00}$ in (15)–(18) can be found in [28], [31], and [39]–[41], and their derivation is not repeated here.

For the QS case and for $\mathbf{r} = \mathbf{r}_{00}$, one has

$$f_{pq}(z) = \sum_{\pm} e^{\pm jk_{z,pq}|z|}\mathrm{erfc}\left(\alpha^{\pm}_{pq}\right)$$

$$\alpha^{\pm}_{pq} = \frac{jk_{z,pq}}{2E} \pm |z|E,$$

$$k_{z,pq} = \sqrt{-\mathbf{k}_{t,pq}\cdot\mathbf{k}_{t,pq}} \tag{19}$$

$$f(R_{mn}) = 2\mathrm{erfc}(R_{mn}E)$$

$$\breve{G}^{\infty}_{00} = \frac{1}{8\pi}f'(0) \tag{20}$$

$$\underline{\mathbf{F}}_{\mathrm{spectral}}(z) = f_{pq}(z)\mathbf{k}_{t,pq}\mathbf{k}_{t,pq} + jf'_{pq}(z)(\mathbf{k}_{t,pq}\hat{\mathbf{z}} + \hat{\mathbf{z}}\mathbf{k}_{t,pq}) - f''_{pq}(z)\hat{\mathbf{z}}\hat{\mathbf{z}} \tag{21}$$

$$\underline{\mathbf{F}}_{\mathrm{spatial}}(R_{mn}) = \left(\frac{f'(R_{mn})}{R^2_{mn}} - \frac{f(R_{mn})}{R^3_{mn}}\right)\underline{\mathbf{I}} + \left(\frac{f''(R_{mn})}{R_{mn}} - \frac{3f'(R_{mn})}{R^2_{mn}} + \frac{3f(R_{mn})}{R^3_{mn}}\right)\hat{\mathbf{R}}_{mn}\hat{\mathbf{R}}_{mn},$$

$$\nabla\nabla\breve{G}^{\infty}_{00} = \frac{1}{24\pi}f'''(0)\underline{\mathbf{I}}. \tag{22}$$

The Ewald method is very convenient here since it provides both rapid converging summations (i.e., only a handful of summation terms is needed to achieve convergence) and analytic continuation to the complex wavevector-plane. The singular terms in (20) and (22) can be determined following the approach in [31], and their evaluation is not repeated here for brevity.

IV. ARRAY OF SRRS IN THE GIGAHERTZ RANGE

In this section, we consider an array of SRRs made of copper whose conductivity is $\sigma = 5.8\times10^7$ S/m that are embedded in free space (i.e., $k = k_0$) and arranged in a square lattice with periodicities $d_x = d_y = 40$ mm. We assume realistic SRR dimensions reported in [19] for flat SRRs with radius $a = 11$ mm, width $w = 0.8$ mm, thickness $h = 0.2$ mm, and gap size $g = 2$ mm. These dimensions make the SRRs resonant at $\omega_0/(2\pi) = 2.1$ GHz [19]. Using the formulas in Section II, one can retrieve the self-inductance $L = 46.91$ nH and the loss resistance $R_l = 413.16$ mΩ at 2.1 GHz.

First, we analyze reflection and transmission coefficients of a 2D periodic array of SRRs as in Fig. 1(a) comparing the SDA with a full-wave method, showing that the SDA method catches pretty well the resonance behavior of the array of SRRs.

Second, using the SDA, we compute the modes with real and complex wavenumber traveling in the same 2D periodic array along one principal axis of the array, say the x-direction, i.e., $\mathbf{k}_{\mathrm{B}} = k_x\hat{\mathbf{x}}$, with $k_x = \beta_x - j\alpha_x$. In other words, we impose $k_y = 0$ for any given frequency and solve $A_{zz}(\mathbf{k}_{\mathrm{B}}) = 0$ in (9) for complex k_x. This assumption can be done without loss of generality and will not affect the conclusions given in this paper.

A. Reflection and Transmission Coefficients

We consider an array of rings with axis along $\hat{\mathbf{v}} = \hat{\mathbf{z}}$, illuminated by a TE-polarized plane wave incident at 30° and 60° from the normal, with H field in the x–z plane, and E field polarized along y. We compare in Fig. 2 results from two different methods: i) the SDA (summarized in Appendix B) and

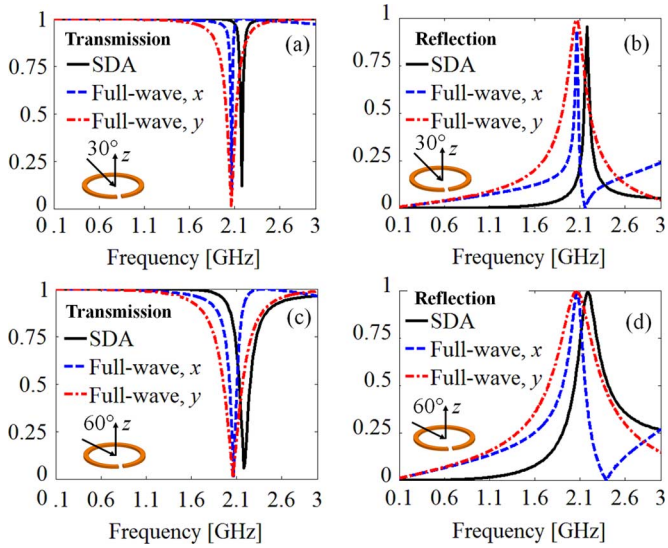

Fig. 2. Magnitude of (a), (c) transmission and (b), (d) reflection coefficients of a 2D periodic array of SRRs in the x–y plane in Fig. 1(a) illuminated by a TE-polarized plane wave incident from (a), (b) 30° and (c), (d) 60°. Regarding the full-wave simulations, each SRR gap is aligned along the direction in the legend. Results show that the SDA method catches the resonant behavior of the SRR array.

ii) full-wave simulations based on the finite-element method in the frequency domain [Microwave Studio by Computer Simulation Technology (CST) Inc.]. We perform two full-wave simulations, one by aligning the gap of each planar SRR along the x-direction, and the other by aligning the gap along the y-direction. [For clarity, by gap aligned along the y-direction, we mean exactly as shown in Fig. 1(a).] The simulation with gap aligned along x avoids direct electric excitation of the SRR because the electric field is polarized along y. Hence, only the magnetic field will excite the SRR. In the case of the gap aligned along y instead, the SRR is excited also by the incident electric field, besides the magnetic field excitation. We note that since the SDA models only magnetic effects, we expect better agreement with full-wave simulations when the gap is aligned along x (full-wave, x) and is thus not excited by the electric field. Moreover, since the array under analysis is not very subwavelength as $d_x = d_y \approx \lambda_0/3.6$ (λ_0 is the free-space wavelength at ω_0), multipolar contributions may also come into play, which are, however, neglected in our SDA model.

Looking at the *transmission plots* in Fig. 2(a) and (c), one may infer that the array of SRRs behaves as a stop-band filter around the SRR resonance at 2.1 GHz (we recall that the complementary structure of the one described here, i.e., a metal plate with SRR-like apertures, would behave as a pass-band filter according to Babinet's principle [42], [43]). Note the agreement between the full-wave and SDA methods for the estimation of the resonance around 2.1 GHz. As mentioned previously, the agreement is better when the electric field does not excite the gap, i.e., when the gap is aligned along x (blue dashed curve). Indeed, when compared with this case, the SDA estimates a transmission resonance bandwidth in good agreement with the full-wave result. When the gap is aligned along y (red dashed–dotted curve), both reflection and transmission exhibit a slightly wider resonance behavior compared with those from the SDA (solid black curve), due to the SRR coupling with the electric field. This wider band, and hence smaller resonance quality factor, is in agreement with the experimental results shown in [44]. This fact can also be noticed by looking at the *reflection plots* in Fig. 2(b) and (d): a reflection dip, signature of a narrow magnetic resonance, is present at around 2.2 GHz (30°) and 2.4 GHz (60°) when the SRR gap is aligned along x. However, this dip disappears when the SRR gap is aligned along y. We note that this dip is not found when using the SDA method, and we attribute this fact to the not very subwavelength dimensions of the array cells, for which multipolar contributions might contribute to the array response [45]. A slight frequency shift towards higher frequencies with respect to the full-wave results is observed in the SDA case (black solid curve). This shift is due to the fact that, in the SDA, we use a quasi-static approximation (2) for the SRR polarizability, and it has been observed also elsewhere, for instance, in [29] for an array of plasmonic nanospheres. Finally, comparing the results for the two considered angles of incidence (30° and 60°), one can notice a larger filtering frequency band as well as a slightly smaller (larger) transmission (reflection) value at resonance for increasing angle, in agreement with [46]. In summary, we have found that the SDA is in fairly good agreement with full-wave simulations and is thus well suited to model waves in arrays even with the SRR radii and inter-resonator distances considered here.

B. Modes With Real and Complex Wavenumber

Assuming that modes are excited by a point source close to the origin, we define as "physical" the modes excitable by the source, similarly to what was done in [27], [28], [36], and [37]. Therefore, for an observer along the positive (negative) x-direction, physical modes are those whose wavenumbers verify the conditions in Table I and have $\alpha_x > 0$ ($\alpha_x < 0$), and thus could propagate in the array without violating energy conservation. In the following, we will assume the observer to be along the positive x direction. The dispersion diagrams (limited to modes with $\alpha_x > 0$) for the array in Section IV-A are shown in Fig. 3(a) and (b) for both β_x and α_x of the wavenumber $k_x = \beta_x - j\alpha_x$ with respect to the angular frequency normalized to the SRR resonance one [we recall that $\omega_0/(2\pi) = 2.1$ GHz]. We show curves computed by using the GF with field retardation (FR) effects (7) and those computed with the QS GF (8); in this subsection, we describe the modal evolution for the more accurate FR case and postpone the discussion of the approximated QS case to the next subsection. Note that here, as was done for the results in Fig. 2, we include ohmic losses modeled by the resistance R_l in (3) (whose value has been given in Section IV) as well as the radiation damping (radiation loss) in (2) in the computation of modal results.

In Fig. 3, we note the presence of two modes at low frequency, namely modes 1 and 2 (blue and green curves, respectively). When looking at the results in Fig. 3, we note a certain similarity with the dispersion diagrams reported in Figs. 11 and 12 in [28] for an array of plasmonic nanospheres. More importantly, we observe similar features with the results reported in [10, Fig. 11(a)] that are relative to the two proper modes in Fig. 3(a) around $0.99 < \omega/\omega_0 < 1.05$ (solid green and blue lines). Note that in [10], losses were not accounted for when evaluating the dispersion relation of 2D arrays of SRRs and that the presence of the improper modes (dashed blue and green lines) was not reported. The method described here allows for the estimation of the complex wavenumbers of both proper and improper as well as both physical and unphysical modes, as detailed in what follows.

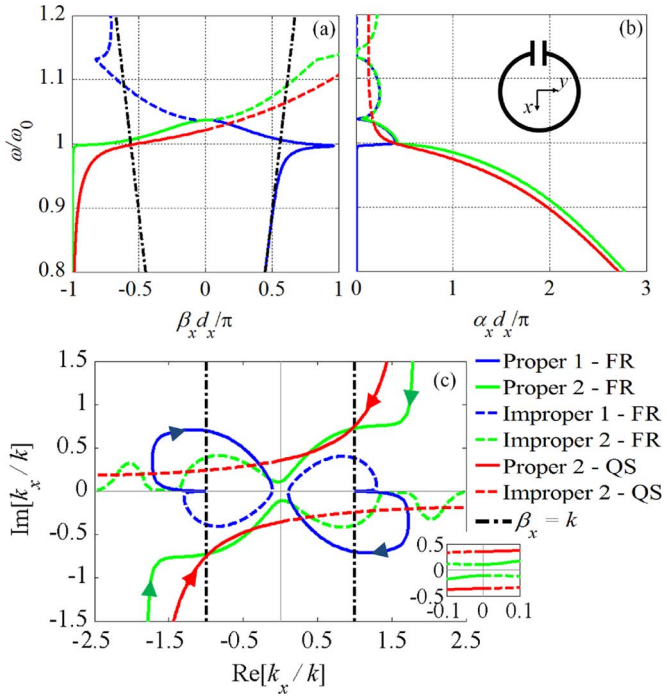

Fig. 3. Dispersion diagram for (a) β_x and (b) α_x of the wavenumber $k_x = \beta_x - j\alpha_x$ for the array in Section IV-A [$\omega_0/(2\pi) = 2.1$ GHz]. (c) Complex plane $\mathrm{Re}[k_x], \mathrm{Im}[k_x]$ normalized by k. The inset shows a zoomed section where the wavenumbers cross from III (I) quadrant (where the modes are proper, solid lines) to IV (II) quadrant (where the modes are improper, dashed lines) of the complex plane for increasing frequency. Arrows indicate the direction of increasing frequency. FR = field retardation, QS = quasi-static.

At low frequencies, mode 1 is a physical forward proper bound mode with β_x close to the light line and small α_x ("Proper 1", solid blue curve). Increasing frequency, this mode deviates from the light line approaching (but not reaching) the edge of the Brillouin zone $\beta_x d_x/\pi = 1$, with increasing α_x. Then, this mode wavenumber experiences a decrease in β_x first with peaking and then decreasing α_x, reaching a small β_x propagation with small α_x. However, when $|\beta_x| < k$, this mode becomes a proper leaky forward mode, unphysical according to Table I. Close to a minimum for β_x, the imaginary part of this mode becomes positive and this mode transitions to the improper mode "Improper 1" [Fig. 3(c), I quadrant] that cannot propagate when the observer is along the positive x direction. The corresponding opposite solution in the III quadrant [dashed blue curve in Fig. 3] is instead a propagating solution, though it is still unphysical because backward *improper* modes cannot be excited according to Table I. One should note the $\pm\mathbf{k}_\mathrm{B}$ symmetry in Fig. 3(c), whereas, in general, solutions are not at $\pm\mathbf{k}_\mathrm{B}^*$, though they may appear close because losses are not very large. Thus, note also that the solution with negative β_x and positive α_x associated with the complex conjugate solution of the mode "Proper 1" is not present, though "Proper 2" (solid green curve) almost satisfies the conjugate condition for certain frequency ranges, as shown in Fig. 3(c).

At low frequencies, mode 2 is a physical backward proper bound mode with almost constant negative value of β_x and decreasing α_x ("Proper 2", solid green curve). Increasing frequency, this mode has a wavenumber whose real part β_x crosses the light line with decreasing α_x, becoming a physical backward leaky mode (solid green curve). Further increasing frequency, β_x goes from negative to positive without changing the sign of α_x, i.e., it goes from the III to IV quadrant of the complex plane in Fig. 3(c) (as is also clearly visible from the inset in the same figure) transitioning into the mode "Improper 2", a physical improper forward leaky mode (dashed green curve). Further increasing frequency, the real part β_x crosses the light line, and this mode becomes an improper bound forward mode, which is unphysical according to Table I. A peculiarity of the dispersion diagram in Fig. 3 is that while at low frequencies, two bound modes—one backward and one forward—are physical and in principle excitable, when frequency is increased such that the wavenumbers are in the region $|\beta_x| < k$, only one leaky mode—either backward or forward—pertaining to mode 2, is physical and excitable.

The result in Fig. 3 clearly shows that efficient waveguides and antennas can be designed by using 2D periodic arrays of SRRs because the physical modes exhibit a very small attenuation constant α_x in certain frequency bands, which allows for either long propagation distances or directive radiation. For example, a potential waveguide could be efficiently designed by employing the proper forward mode 1 for $\omega/\omega_0 < 1$. Moreover, a potential leaky wave antenna could be efficiently designed by employing either the proper backward mode 2 or the improper forward mode 2. In particular, we note that in this configuration (i.e., an array of rings with axis along $\hat{\mathbf{v}} = \hat{\mathbf{z}}$), the magnetic dipoles modeling the SRRs have a radiation null along the z-direction. This means that the choice of a mode around $\omega/\omega_0 \approx 1.04$, which would in principle radiate at broadside, will not result in efficient radiation. The use of modes below or above $\omega/\omega_0 \approx 1.04$ in Fig. 3, with β_x far from 0 or close to the light line, results in radiation away from broadside or even in the endfire condition. However, further engineering of modal dispersion is required to reduce α_x in such frequency regions to optimize radiation directivity. To conclude, note also that other modes are present in the present configuration but not reported because they have large attenuation constant α_x.

C. Discussion: Electrodynamic Modes and Magnetostatic Waves

In Section IV-B, we have discussed the physical modes excitable by a localized source, a defect, or array truncation using the FR GF model for fields generated by every magnetic dipole. As stated in Section II, the QS model may also be adopted to evaluate the modal wavenumbers, as was done in several previous papers. This model is a good approximation in the case of very subwavelength array element spacings. The dispersion diagrams for the array in Section IV-A employing the QS GF magnetic dipole model are shown in Fig. 3 (red curves). It is noteworthy that only the presence of mode 2 is predicted, and no evidence of the presence of mode 1 is found. Moreover, the QS model provides only the salient propagation characteristics of mode 2 and hinders the frequency bands with very small α_x. In conclusion, the result in Fig. 3 applied to an array with periods $d_x = d_y \approx \lambda_0/3.6$ shows the importance of considering the FR solution versus the QS one because the QS model is not capable of predicting propagation of mode 1 and does not describe well the dispersion of mode 2.

V. Modes in a Deeply Subwavelength 2D Periodic Array of Capacitively Loaded Loops

Following our previous discussion in Section IV-C, in this section, we will show the results of mode propagation in deeply subwavelength arrays of capacitively loaded loops using the two

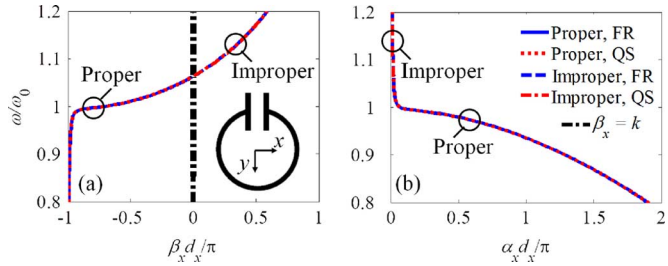

Fig. 4. Dispersion diagram for an array of capacitively loaded loops where the direction orthogonal to the ring plane is $\hat{\mathbf{v}} = \hat{\mathbf{z}}$ as in Fig. 1(a) [$\omega_0/(2\pi) = 63.87$ MHz]. The light line is almost vertical because the period is deeply subwavelength.

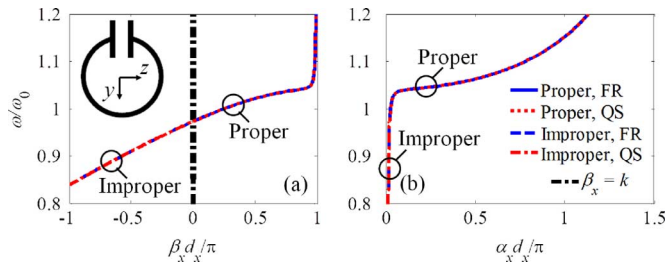

Fig. 5. Dispersion diagram for an array of capacitively loaded loops where the direction orthogonal to the ring plane is $\hat{\mathbf{v}} = \hat{\mathbf{x}}$ as in Fig. 1(b) [$\omega_0/(2\pi) = 63.87$ MHz].

GF models adopted in Section IV. We expect the two models to provide results in very good agreement because the subwavelength condition satisfies the QS assumption.

We analyze modes with real and complex wavenumber traveling along the x-direction with $\mathbf{k}_\mathrm{B} = k_x\hat{\mathbf{x}}$, where $k_x = \beta_x - j\alpha_x$ (assuming an observer along the positive x-direction). We consider 2D periodic arrays of capacitively loaded loops embedded in free space (i.e., $k = k_0$), for the three loop orientations in Fig. 1(a)–(c), arranged in a square lattice with periodicities $d_x = d_y = 23$ mm. The use of a lumped capacitor largely lowers the resonance frequency of the loop, making the array deeply subwavelength with respect to the free-space wavelength. This characteristic can be observed by the fact that the light line in the dispersion diagrams in Figs. 4–6 is almost a vertical line, in contrast to the case described in Fig. 3. We observe similar features to the dispersion diagrams reported in Figs. 11 and 12 in [28] for an array of plasmonic nanospheres. Moreover, the use of a lumped capacitor allows for an easy tunability of the loop resonance frequency. We use copper loops with the following characteristics: $L = 33$ nH, $C = 188$ pF, $Q = \sqrt{L/C}/R = 200$, $\omega_0/(2\pi) = 63.87$ MHz, as in [22], and thus $d_x = d_y \approx \lambda_0/204$; a practical design for the loops would be $r \approx 8.47$ mm, $w \approx 0.826$ mm, $h \ll w$ and $R_l = 67.17$ mΩ at 63.87 MHz, achieved using the formulas reported in Section II.

A. Loops With Axis Along the z-Direction (T-Pol)

The dispersion diagrams (limited to modes with $\alpha_x > 0$) for an array as in Fig. 1(a), where the direction orthogonal to the ring plane is $\hat{\mathbf{v}} = \hat{\mathbf{z}}$, are shown in Fig. 4 for both β_x and α_x of the wavenumber $k_x = \beta_x - j\alpha_x$ with respect to the angular frequency normalized to the SRR resonance one [we recall that $\omega_0/(2\pi) = 63.87$ MHz]. Therefore, each magnetic dipole moment is polarized transversely with respect to the direction of propagation (T-pol). At low frequency, the mode "Proper" is a backward physical proper bound mode with an almost constant negative value of β_x and decreasing α_x. Increasing frequency, this mode has a wavenumber whose real part β_x crosses the light line (β_x is still negative), thus becoming a physical backward leaky mode (although this is a condition that happens for a very narrow bandwidth due to the deep subwavelength condition). When β_x goes from negative to positive without changing the sign of α_x (i.e., crossing from III to IV quadrant of the complex plane), this mode transitions to the forward mode "Improper", which is physical and leaky when $\beta_x < k$ and becomes unphysical and bound when $\beta_x > k$. When physical, this mode exhibits also a small α_x for a small frequency band for both bound and leaky conditions, and thus it is a good candidate for both waveguiding and radiation purposes. In particular, the forward improper leaky mode around $\omega/\omega_0 \approx 1.06$ in Fig. 4 provides directive radiation away from broadside and even in the endfire condition thanks to the small attenuation constant α_x. Note that this mode has very high attenuation constant for $\omega < \omega_0$ and starts to be able to propagate along the array for $\omega > \omega_0$, i.e., when magnetic energy is predominantly stored in the loops.

The modes evaluated with the QS approximations are found in good agreement with dynamic case (FR). To conclude, note also that other modes are present, but not reported, because they exhibit larger attenuation constant α_x.

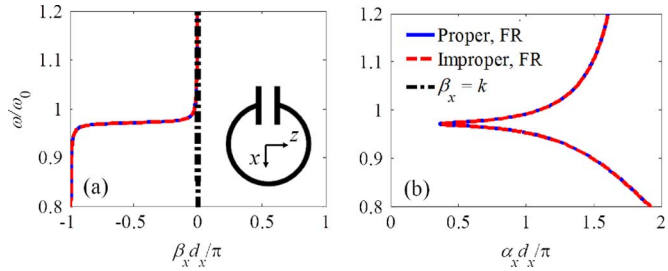

Fig. 6. Dispersion diagram for an array of capacitively loaded loops where the direction orthogonal to the ring plane is $\hat{\mathbf{v}} = \hat{\mathbf{y}}$ as in Fig. 1(c) [$\omega_0/(2\pi) = 63.87$ MHz]. Due to clarity of the figure, we report only the proper and improper solutions computed using the FR GF. Perfectly overlapping curves can be calculated using the QS GF.

B. Loops With Axis Along the x-Direction (L-Pol)

In Fig. 5, we show dispersion diagrams similar to those in Fig. 4, but now for the array in Fig. 1(b), where the direction orthogonal to the ring plane is $\hat{\mathbf{v}} = \hat{\mathbf{x}}$. Therefore each magnetic dipole moment is polarized longitudinally with respect to the direction of propagation (L-pol).

At low frequency, the mode "Improper" is a backward unphysical improper mode with increasing β_x and increasing α_x. When β_x goes from negative to positive without changing the sign of α_x (i.e., crossing from the III to IV quadrant of the complex plane), this mode transitions to the mode "Proper", a proper forward mode, physical and bound when $\beta_x > k$. In particular, this physical mode exhibits a small α_x for $\omega < \omega_0$, but there it is unphysical for $\beta_x < 0$. It also exhibits a low attenuation constant in a small frequency region for $\omega > \omega_0$, and for $\beta_x > k$ is physical, and thus it can be excited. In this small frequency region, it can be used for forward propagation.

Note that this mode, in general, has very high attenuation constant for $\omega > \omega_0$, in contrast to the case in Fig. 4. It is able to propagate along the array for $\omega < \omega_0$, i.e., when electric energy is predominantly stored in the loops.

Notice also that other modes are present, but not reported, because they are largely attenuated. No backward propagation with moderately low attenuation is found in this case. The modes evaluated with the QS approximations are found in good agreement with dynamic case (FR).

C. Loops With Axis Along the y-Direction (T-Pol)

We show in Fig. 6 the dispersion diagrams, similarly to what we did in Fig. 4, but now for the array in Fig. 1(c), where the direction orthogonal to the ring plane is $\hat{\mathbf{v}} = \hat{\mathbf{y}}$. Therefore, each magnetic dipole moment is polarized transversely with respect to the direction of propagation (T-pol). At low frequency, the mode "Proper" is a backward physical proper bound mode with increasing β_x and decreasing α_x. A minimum normalized attenuation constant of about 0.4 is reached in the resonant region, at an angular frequency slightly smaller than ω_0. At high frequency, the mode is still proper, physical and backward, and has high attenuation constant. The mode "Improper", an unphysical improper mode, is found to have a propagation constant almost on top of the one of the proper mode.

Notice also that other modes are present, but not reported, because they are largely attenuated. No forward propagation with moderately low attenuation is found in this case. The modes evaluated with the QS approximations are found in good agreement with dynamic case (FR).

VI. Conclusion

The strength of our analysis is that it allows for a comprehensive characterization of the modal wavenumbers according to proper, improper, forward, backward, bound, and leaky conditions. This, in turn, allows for the determination of the physical and unphysical modes excitable by a localized source, a defect, or array truncation. This enables the use of the described method for designing waveguiding or radiating structures based on magnetoinductive waves. We have shown that modal wavenumber features are well described by magnetoinductive waves, under the QS approximation, in deeply subwavelength SRR arrays, as shown in Section V. In contrast, only salient propagation characteristics are achieved when the array dimensions are comparable to the SRR resonance wavelength in comparison to the case when field retardation is accounted for, as shown in Section IV. In this latter case, the QS approximation totally misses the description of some other mode.

Appendix A
Derivation of the Ewald Representation for the Quasi-Static Green's Function

We summarize here the steps to obtain the Ewald representation for the quasi-static dyadic Green's function to be used in (5). According to [39] and [47], one can write

$$\frac{1}{R_{mn}} = \frac{2}{\sqrt{\pi}} \int_0^\infty e^{-R_{mn}^2 s^2}\, ds. \tag{23}$$

Then, by splitting the integral in (23) into the summation $\int_0^\infty = \int_0^E + \int_E^\infty$, with $E = \sqrt{\pi/(d_x d_y)}$ being the Ewald parameter, the first integral represents the spectral term, and the second one the spatial term. Following the steps in [31] and [39], one can easily express the spectral terms as in Section III, with $k_{z,pq} = \sqrt{-\mathbf{k}_{t,pq} \cdot \mathbf{k}_{t,pq}}$. Moreover, according to [39] and [47], one can write

$$\frac{2}{\sqrt{\pi}} \int_E^\infty e^{-R_{mn}^2 s^2}\, ds = \frac{\operatorname{erfc}(R_{mn} E)}{R_{mn}} \tag{24}$$

which allows for the retrieval of the spatial terms in Section III. Interestingly, these expressions can be also obtained by evaluating the formulas in [31] and [39] with $k = 0$.

Appendix B
Retrieval of Reflection and Transmission Coefficients Using the Single Dipole Approximation

In general, it is possible to compute the induced magnetic dipole moment m_{00} by solving the scalar equation in (9) in the case of a 2D periodic array illuminated by a TE-polarized incident plane wave that evaluated at the origin is $\mathbf{H}_{\mathrm{PW}}^{\mathrm{inc}} = H_{\mathrm{PW}}^{\mathrm{inc}}(\cos\theta\hat{\mathbf{x}} + \sin\theta\hat{\mathbf{z}})$ with θ being the incident angle and $H_{\mathrm{PW}}^{\mathrm{inc}}$ the plane wave magnitude. The scattered magnetic field $\mathbf{H}_{\mathrm{PW}}^{\mathrm{s}}$ produced by such an illumination is then calculated as

$$\mathbf{H}_{\mathrm{PW}}^{\mathrm{s}}(\mathbf{r}, \mathbf{r}_{00}, \mathbf{k}_t) = \underline{\mathbf{G}}_{\mathrm{PW}}^{\infty}(\mathbf{r}, \mathbf{r}_{00}, \mathbf{k}_t) \cdot \mathbf{m}_{00} \tag{25}$$

where $\mathbf{k}_t = k_x\hat{\mathbf{x}} + k_y\hat{\mathbf{y}}$ is the transverse part of the plane wave wavenumber $\mathbf{k} = k_x\hat{\mathbf{x}} + k_y\hat{\mathbf{y}} \pm k_z\hat{\mathbf{z}}$, where the plus (minus) sign is used when the observation point $\mathbf{r}$ is above (below) the array plane, and $k_z = \sqrt{k^2 - k_x^2 - k_y^2}$. The term $\underline{\mathbf{G}}_{\mathrm{PW}}^{\infty}(\mathbf{r}, \mathbf{r}_{00}, \mathbf{k}_t)$ is computed as

$$\underline{\mathbf{G}}_{\mathrm{PW}}^{\infty}(\mathbf{r}, \mathbf{r}_{00}, \mathbf{k}_t) = \frac{e^{-j\mathbf{k}_t \cdot (\mathbf{r} - \mathbf{r}_{00})} e^{-jk_z |z - z_{00}|}}{2jd_x d_y k_z} [k^2 \underline{\mathbf{I}} - \mathbf{k}\mathbf{k}] \tag{26}$$

assuming that only the 00th Floquet component is within the first Brillouin zone, implying that d_x, d_y are shorter than half-wavelength. Then, reflection and transmission coefficients from the array are evaluated as

$$\Gamma = -\frac{\mathbf{H}_{\mathrm{PW}}^{\mathrm{s},+} \cdot \hat{\mathbf{x}}}{\mathbf{H}_{\mathrm{PW}}^{\mathrm{inc}} \cdot \hat{\mathbf{x}}}, \quad T = 1 + \frac{\mathbf{H}_{\mathrm{PW}}^{\mathrm{s},-} \cdot \hat{\mathbf{x}}}{\mathbf{H}_{\mathrm{PW}}^{\mathrm{inc}} \cdot \hat{\mathbf{x}}} \tag{27}$$

where $\mathbf{H}_{\mathrm{PW}}^{\mathrm{s},+}$ and $\mathbf{H}_{\mathrm{PW}}^{\mathrm{s},-}$ are scattered magnetic fields from the 2D array of SRRs above and below the array plane referred to the array plane, respectively.

Acknowledgment

The authors acknowledge Dr. S. Steshenko, Institute of Radiophysics and Electronics of the National Academy of Sciences of Ukraine and University of Siena, Italy, for fruitful discussions. The authors also thank CST Inc. for providing CST Microwave Studio that was instrumental in this work.

References

[1] D. R. Smith, W. J. Padilla, D. C. Vier, S. C. Nemat-Nasser, and S. Schultz, "Composite medium with simultaneously negative permeability and permittivity," *Phys. Rev. Lett.*, vol. 84, pp. 4184–4187, May 2000.

[2] S. Hrabar, Z. Eres, and J. Bartolic, "Capacitively loaded loop as basic element of negative permeability meta-material," in *Proc. 32nd Eur. Microw. Conf.*, 2002, pp. 1–4.

[3] K. Aydin and E. Ozbay, "Capacitor-loaded split ring resonators as tunable metamaterial components," *J. Appl. Phys.*, vol. 101, p. 024911-5, Jan. 2007.

[4] M. J. Freire and R. Marques, "Planar magnetoinductive lens for three-dimensional subwavelength imaging," *Appl. Phys. Lett.*, vol. 86, pp. 182505–3, Apr. 2005.

[5] M. J. Freire and R. Marques, "Near-field imaging in the megahertz range by strongly coupled magnetoinductive surfaces: Experiment and ab initio analysis," *J. Appl. Phys.*, vol. 100, pp. 063105–9, Sept. 2006.

[6] M. J. Freire and R. Marques, "Optimizing the magnetoinductive lens: Improvement, limits, and possible applications," *J. Appl. Phys.*, vol. 103, pp. 013115–7, Jan. 2008.

[7] K. Bartusek, P. Drexler, P. Fiala, R. Kadlec, and R. Kubasek, "Magnetoinductive lens for experimental mid-field MR tomograph," *PIERS Online*, vol. 6, pp. 621–624, 2010.

[8] R. Marques, L. Jelinek, M. J. Freire, J. D. Baena, and M. Lapine, "Bulk metamaterials made of resonant rings," *Proc. IEEE*, vol. 99, pp. 1660–1668, Oct. 2011.

[9] C. J. Stevens, C. W. T. Chan, K. Stamatis, and D. J. Edwards, "Magnetic metamaterials as 1-D data transfer channels: An application for magneto-inductive waves," *IEEE Trans. Microw. Theory Technol.*, vol. 58, pp. 1248–1256, May 2010.

[10] E. Shamonina, V. A. Kalinin, K. H. Ringhofer, and L. Solymar, "Magnetoinductive waves in one, two, and three dimensions," *J. Appl. Phys.*, vol. 92, pp. 6252–6261, Aug. 2002.

[11] I. V. Shadrivov, A. N. Reznik, and Y. S. Kivshar, "Magnetoinductive waves in arrays of split-ring resonators," *Physica B, Condens. Matter*, vol. 394, pp. 180–183, May 2007.

[12] R. R. A. Syms, I. R. Young, and L. Solymar, "Low-loss magneto-inductive waveguides," *J. Phys. D, Appl. Phys.*, vol. 39, p. 3945, Sept. 2006.

[13] M. C. K. Wiltshire, E. Shamonina, I. R. Young, and L. Solymar, "Experimental and theoretical study of magneto-inductive waves supported by one-dimensional arrays of "swiss rolls"," *J. Appl. Phys.*, vol. 95, pp. 4488–4493, Jan. 2004.

[14] M. C. K. Wiltshire, E. Shamonina, I. R. Young, and L. Solymar, "Dispersion characteristics of magneto-inductive waves: comparison between theory and experiment," *Electron. Lett.*, vol. 39, pp. 215–217, Jan. 2003.

[15] V. Lomanets, O. Zhuromskyy, G. Onishchukov, O. Sydoruk, E. Tatartschuk, E. Shamonina, G. Leuchs, and U. Peschel, "Interacting waves on chains of split-ring resonators in the presence of retardation," *Appl. Phys. Lett.*, vol. 97, pp. 011108–3, July 2010.

[16] A. Radkovskaya, O. Sydoruk, M. Shamonin, E. Shamonina, C. J. Stevens, G. Faulkner, D. J. Edwards, and L. Solymar, "Experimental study of a bi-periodic magnetoinductive waveguide: comparison with theory," *IET Microw. Antennas Propag.*, vol. 1, pp. 80–83, Feb. 2007.

[17] O. Sydoruk, O. Zhuromskyy, E. Shamonina, and L. Solymar, "Phonon-like dispersion curves of magnetoinductive waves," *Appl. Phys. Lett.*, vol. 87, p. 072501-3, Aug. 2005.

[18] O. Sydoruk, A. Radkovskaya, O. Zhuromskyy, E. Shamonina, M. Shamonin, C. J. Stevens, G. Faulkner, D. J. Edwards, and L. Solymar, "Tailoring the near-field guiding properties of magnetic metamaterials with two resonant elements per unit cell," *Phys. Rev. B*, vol. 73, p. 224406-12, June 2006.

[19] F. Hesmer, E. Tatartschuk, O. Zhuromskyy, A. A. Radkovskaya, M. Shamonin, T. Hao, C. J. Stevens, G. Faulkner, D. J. Edwards, and E. Shamonina, "Coupling mechanisms for split ring resonators: Theory and experiment," *Phys. Status Solidi B-Basic Solid State Phys.* , vol. 244, pp. 1170–1175, Apr. 2007.

[20] O. Zhuromskyy, O. Sydoruk, E. Shamonina, and L. Solymar, "Slow waves on magnetic metamaterials and on chains of plasmonic nanoparticles: Driven solutions in the presence of retardation," *J. Appl. Phys.*, vol. 106, pp. 104908–7, Nov. 2009.

[21] K. Aydin and E. Ozbay, "Experimental investigation of reflection characteristics of left-handed metamaterials in free space," *IET Microw. Antennas Propag.*, vol. 1, pp. 89–93, Feb. 2007.

[22] O. Sydoruk, O. Zhuromskyy, A. Radkovskaya, E. Shamonina, and L. Solymar, "Magnetoinductive waves I: Theory," in *Theory and Phenomena of Metamaterials*, F. Capolino, Ed. Boca Raton, FL, USA: CRC Press, 2009, p. 36.1.

[23] O. Z. O. Sydoruk, A. Radkovskaya, E. Shamonina, and L. Solymar, "Magnetoinductive waves II: Application," in *Applications of Metamaterials*, F. Capolino, Ed. Boca Raton, FL, USA: CRC Press, 2009, p. 14.1.

[24] E. Tatartschuk, A. Radkovskaya, E. Shamonina, and L. Solymar, "Generalized Brillouin diagrams for evanescent waves in metamaterials with interelement coupling," *Phys. Rev. B*, vol. 81, p. 115110-10, Mar. 2010.

[25] R. Arias and D. L. Mills, "Theory of collective spin waves and microwave response of ferromagnetic nanowire arrays," *Phys. Rev. B*, vol. 67, p. 094423-15, Mar. 2003.

[26] E. Shamonina, "Magnetoinductive polaritons: Hybrid modes of metamaterials with interelement coupling," *Phys. Rev. B*, vol. 85, p. 155146-10, Apr. 2012.

[27] S. Campione, S. Steshenko, and F. Capolino, "Complex bound and leaky modes in chains of plasmonic nanospheres," *Opt. Express*, vol. 19, pp. 18345–18363, Sep. 2011.

[28] A. L. Fructos, S. Campione, F. Capolino, and F. Mesa, "Characterization of complex plasmonic modes in two-dimensional periodic arrays of metal nanospheres," *J. Opt. Soc. Amer. B*, vol. 28, pp. 1446–1458, June 2011.

[29] S. Steshenko and F. Capolino, "Single dipole approximation for modeling collection of nanoscatterers," in *Theory and Phenomena of Metamaterials*, F. Capolino, Ed. Boca Raton, FL, USA: CRC Press, 2009, p. 8.1.

[30] C. F. Bohren and D. R. Huffman, *Absorption and Scattering of Light by Small Particles*. New York, NY, USA: Wiley, 1983.

[31] S. Steshenko, F. Capolino, P. Alitalo, and S. Tretyakov, "Effective model and investigation of the near-field enhancement and subwavelength imaging properties of multilayer arrays of plasmonic nanospheres," *Phys. Rev. E*, vol. 84, p. 016607-12, Jul. 2011.

[32] R. Marques, F. Martin, and M. Sorolla, *Metamaterials with Negative Parameters*. Hoboken, NJ, USA: Wiley, 2008.

[33] R. Marques, F. Mesa, J. Martel, and F. Medina, "Comparative analysis of edge- and broadside—Coupled split ring resonators for metamaterial design—Theory and experiments," *IEEE Trans. Antennas Propag.*, vol. 51, pp. 2572–2581, Oct. 2003.

[34] R. Marqués, J. D. Baena, M. Beruete, F. Falcone, T. Lopetegi, M. Sorolla, F. Martín, and J. Garcia, "Ab initio analysis of frequency selective surfaces based on conventional and complementary split ring resonators," *J. Opt. A, Pure Appl. Opt.*, vol. 7, pp. S38–S43, Jan. 2005.

[35] B. Sauviac, C. R. Simovski, and S. A. Tretyakov, "Double split-ring resonators: Analytical modeling and numerical simulations," *Electromagnetics*, vol. 24, pp. 317–338, Jul. 2004.

[36] P. Baccarelli, S. Paulotto, and C. D. Nallo, "Full-wave analysis of bound and leaky modes propagating along 2d periodic printed structures with arbitrary metallisation in the unit cell," *IET Microw. Antennas Propag.*, vol. 1, pp. 217–225, Feb. 2007.

[37] F. Capolino, D. R. Jackson, and D. R. Wilton, "Field representations in periodic artificial materials excited by a source," in *Theory and Phenomena of Metamaterials*, F. Capolino, Ed. Boca Raton, FL, USA: CRC Press, 2009, p. 12.1.

[38] D. R. Jackson and A. A. Oliner, "Leaky-wave antennas," in *Modern Antenna Handbook*, C. A. Balanis, Ed. New York, NY, USA: Wiley, 2008, pp. 325–367.

[39] K. E. Jordan, G. R. Richter, and P. Sheng, "An efficient numerical evaluation of the Green-function for the Helmholtz operator on periodic structures," *J. Comput. Phys.*, vol. 63, pp. 222–235, Mar. 1986.

[40] S. Oroskar, D. R. Jackson, and D. R. Wilton, "Efficient computation of the 2D periodic Green's function using the Ewald method," *J. Comput. Phys.*, vol. 219, pp. 899–911, Dec. 2006.

[41] F. T. Celepcikay, D. R. Wilton, D. R. Jackson, and F. Capolino, "Choosing splitting parameters and summation limits in the numerical evaluation of 1-D and 2-D periodic Green's functions using the Ewald method," *Radio Sci.*, vol. 43, p. RS6S01-11, Sep. 2008.

[42] F. Falcone, T. Lopetegi, M. A. G. Laso, J. D. Baena, J. Bonache, M. Beruete, R. Marqués, F. Martín, and M. Sorolla, "Babinet principle applied to the design of metasurfaces and metamaterials," *Phys. Rev. Lett.*, vol. 93, p. 197401-4, Nov. 2004.

[43] L. Sahin, K. Aydin, G. T. Sayan, and E. Ozbay, "Enhanced transmission of electromagnetic waves through split-ring resonator-shaped apertures," *J. Nanophotonics*, vol. 5, p. 051812-14, Jun. 2011.

[44] N. Katsarakis, T. Koschny, M. Kafesaki, E. N. Economou, and C. M. Soukoulis, "Electric coupling to the magnetic resonance of split ring resonators," *Appl. Phys. Lett.*, vol. 84, pp. 2943–2945, Feb. 2004.

[45] M. Garcia-Vigueras, F. Mesa, F. Medina, R. Rodriguez-Berral, and J. L. Gomez-Tornero, "Simplified circuit model for arrays of metallic dipoles sandwiched between dielectric slabs under arbitrary incidence," *IEEE Trans. Antennas Propag.*, vol. 60, pp. 4637–4649, Oct. 2012.

[46] M. Jakovljevic, B. Vasic, G. Isic, R. Gajic, T. Oates, K. Hinrichs, I. Bergmair, and K. Hingerl, "Oblique incidence reflectometry and spectroscopic ellipsometry of split-ring resonators in infrared," *J. Nanophotonics*, vol. 5, pp. 051815–10, July 2011.
[47] P. P. Ewald, "The calculation of optical and electrostatic grid potential," *Ann. Phys. Berlin*, vol. 64, pp. 253–287, Feb. 1921.

Salvatore Campione (S'09) received the Laurea triennale degree (*cum laude*) in electrical engineering from Polytechnic of Turin, Turin, Italy, in 2007, the Laurea Magistrale degree (*cum laude*) in electrical engineering from the Polytechnic of Turin, Turin, Italy, in 2009, and the Master of Science degree in electrical engineering from the University of Illinois at Chicago, USA, in 2009.

He is currently working towards the Ph.D. degree at the University of California Irvine, Irvine, CA, USA. He has been at the U.S. Army Charles M. Bowden Research Center, RDECOM, Redstone Arsenal, Huntsville, AL, USA, and at the Center for Integrated Nanotechnologies (CINT) at Sandia National Laboratories, Albuquerque, NM, USA, in 2012. His research interests include metamaterials and their applications, plasmonics in nanostructures, and optical devices with superresolution.

Mr. Campione has been the recipient of a Sigma Xi Grant-in-Aid of Research (2011), two SPIE Scholarships in Optics and Photonics (2011 and 2012), and of several travel grants, including the Newport Spectra Physics Research Excellence Travel Award (2011), granted by SPIE, and the FGSA Travel Award for Excellence in Graduate Research (2012), granted by the American Physical Society.

Francisco Mesa (M'93–SM'11) was born in Cádiz, Spain. He received the Licenciado and Doctor degrees in physics from the University of Sevilla, Sevilla, Spain, in 1989 and 1991, respectively.

He is currently Professor in the Department of Applied Physics 1, University of Sevilla, Seville, Spain. His research interests focus on electromagnetic propagation/radiation in planar structures.

Filippo Capolino (S'94–M'97–SM'04) received the Laurea (*cum laude*) and the Ph.D. degrees in electrical engineering from the University of Florence, Italy, in 1993 and 1997, respectively.

He is currently an Associate Professor at the Department of Electrical Engineering and Computer Science of the University of California, Irvine, CA, USA. He has been an Assistant Professor at the Department of Information Engineering of the University of Siena, Italy. From 1997 to 1999, he was a Postdoctoral Fellow with the Department of Aerospace and Mechanical Engineering, Boston University, MA, USA. From 2000 to 2001 and in 2006, he was a Research Assistant Visiting Professor with the Department of Electrical and Computer Engineering, University of Houston, TX, USA. His research interests include antennas, metamaterials and their applications, sensors in both microwave and optical ranges, wireless systems, chip-integrated antennas. He was the EU Coordinator of the EU Doctoral Programs on Metamaterials from 2004 to 2009.

Dr. Capolino received the R. W. P. King Prize Paper Award from the IEEE Antennas and Propagation Society for the Best Paper of the Year 2000, by an author under 36. He is a coauthor of the "Fast Breaking Papers, Oct. 2007" in Electrical Engineering and Computer Science, about metamaterials [a paper that had the highest percentage increase in citations in Essential Science Indicators (ESI)]. He also received several young and senior scientist travel grants (IEEE and URSI) and two student and young scientist paper competition awards. From 2002 to 2008, he served as an Associate Editor for the IEEE TRANSACTIONS ON ANTENNAS AND PROPAGATION. He is the Editor of the *Metamaterials Handbook* (Boca Raton, FL, USA: CRC Press, 2009).